International Journal of Biological Macromolecules 121 (2019) 77–88

Contents lists available at ScienceDirect

International Journal of Biological Macromolecules

journal homepage: http://www.elsevier.com/locate/ijbiomac

Evaluating the biological properties of synthetic 4-nitrophenyl functionalized benzofuran derivatives with telomeric DNA binding and antiproliferative activities

Antonio Carella [a,1], Valentina Roviello [b,1], Roberta Iannitti [c], Rosanna Palumbo [c], Sara La Manna [d], Daniela Marasco [c,d], Marco Trifuoggi [a], Rosita Diana [a], Giovanni N. Roviello [c,*]

[a] University of Naples Federico II, Department of Chemical Sciences, Via Cintia 21, I-80126 Naples, Italy
[b] Analytical Chemistry for the Environment and CeSMA (Advanced Metrologic Service Center), University of Naples Federico II, Corso N. Protopisani, 80146 Naples, Italy
[c] CNR, Institute of Biostructure and Bioimaging – (Via Mezzocannone Site and Headquarters), 80134 Naples, Italy
[d] University of Naples Federico II, Department of Pharmacy, Via Mezzocannone 16, 80134 Naples, Italy

ARTICLE INFO

Article history:
Received 14 June 2018
Received in revised form 12 September 2018
Accepted 24 September 2018
Available online 25 September 2018

Keywords:
Benzofuran
Nucleic acid-interaction
Prostate cancer
Antiproliferative
Telomeric DNA

ABSTRACT

Four 4-nitrophenyl-functionalized benzofuran (**BF1**, **BF2**) and benzodifuran (**BDF1**, **BDF2**) compounds were synthesized by a convenient route based on the Craven reaction. All the compounds underwent a detailed chemical-physical characterization to evaluate their structural, thermal and optical properties. An investigation on the therapeutic potential of the reported compounds was performed by analyzing their antiproliferative activity on prostatic tumour cells (PC-3). In both classes of compounds, anticancer potential is in direct correlation with the lipophilicity. From our study it emerged that antiproliferative activity was higher for benzofuran derivatives as compared to benzodifuran systems. Moreover, we report a mechanistic study relative to the most promising molecule, i.e. the apolar benzofuran **BF1**, that relates the antiproliferative properties found in our investigation to its ability to bind telomeric DNA (proven by CD and fluorescence techniques on tel_{22} G4 DNA), and highlights its unexpected impact on cell cycle progression.

1. Introduction

Heterocyclic compounds play a very important role in organic chemistry both in relation to their biological activity and for their application in material science; indeed, over the 60% of the top retailing drugs in 2010 contains at least one heterocycle as a part of its molecular backbone [1]. At the same time, organic materials for applications in high technologically demanding fields as nonlinear optics or organic electronics are based on highly polarizable heterocycles [2–5].

In this context, oxygen containing heterocycles represent an important class of compounds exhibiting interesting biological and pharmacological activity, since their similarity to several natural bioactive molecules [6,7]. Benzofuran derivatives have drawn a considerable interest as powerful systems displaying a wide range of biological properties including antimicrobial [8,9], antitumor [10,11], anti-parasitic [12], analgesic activity [13]. Benzofurans can inhibit particular serine/threonine kinases whose aberrations are correlated with cancer development, and decrease the proliferation and colony formation of several cancer cell lines elevating their percentages in the G2/M phase of the cell cycle [11]. Benzodifuran derivatives as well have proved as efficient pharmacological agents with antibacterial/antifungal [9,14], anti-inflammatory [15] and, more recently, antiviral activity [16,17]. Both the classes of heterocyclic compounds (benzofuran and benzodifuran derivatives) have moreover found applications in the field of the industrial dyes as optical whiteners or disperse dyes characterized by high fastness properties. They have also been investigated in different fields of organic electronics and photonics: dyes based on benzofuran heterocycles have shown interesting second order nonlinear optical properties [18] and have been, moreover, used as efficient photosensitizers in dye sensitized solar cells [19]. Benzodifuran derivatives have been reported as efficient photoluminescent materials [20] and have shown excellent semiconducting properties in the field of organic solar cell and transistors where they are prevalently used as electron-rich building blocks in small molecule or polymeric architecture [21]. They have also been used as monomers in the preparation of interesting liquid crystalline polymers [22].

Numerous synthetic approaches were reported for the synthesis of benzofurans, but most of these are associated with transition-metal-catalyzed annulation reactions of pre-functionalized substrates which were typically synthesized by Heck or Sonogashira coupling reactions

* Corresponding author.
E-mail address: giroviel@unina.it (G.N. Roviello).
[1] These authors contributed equally.

https://doi.org/10.1016/j.ijbiomac.2018.09.153
0141-8130/

[23–26]. There are few synthetic methodologies available in this area not requiring transition metals which include cyclization of *o*-hydroxystilbenes using hypervalent iodine compounds [27] or intramolecular photochemical Wittig reaction of functionalized phosphonium bromides [28].

The synthesis of benzodifuran cycles is well established and widely reported in the literature [29]. One of the simplest strategies consists in the reaction of 1,4-benzoquinone with several cyanoacetic esters in alcoholic ammonia, known as Craven reaction [30,31]: the obtained product, 2,6-diaminofuro[2′,3′:4,5]benzo[*b*]furan-3,7-dicarboxylate, derives from a double nucleophilic reaction on the benzoquinone ring. In more recent years Obushak et al. investigated the Craven reaction between a 2-aryl-1,4-benzoquinone and ethyl or methyl cyanoacetate [32]. They observed that the reaction selectively afforded the benzodifuran derivatives, regardless the used reagent ratios. Only in one case, by using the quinone derivative 2-(4-nitrophenyl)-1,4-benzoquinone (**NO2BQ**), minor amounts of benzofuran derivative (ethyl-2-amino-5-hydroxy-4-(4-nitrophenyl)-benzo[*b*]furan-3-carboxylate) were isolated.

The potential employment of a cheap and simple reaction as the Craven reaction for the synthesis of benzofuran derivatives prompted us to further investigate the behavior of **NO2BQ** in this synthetic pathway: the quinone derivative was reacted with two different cyanoacetic esters bearing tails of similar lengths but different flexibility, i.e., butyl-cyanoacetate and 2-methoxyethyl-cyanoacetate: from each reaction we managed to isolate both the benzofuran (**BF**) and (**BDF**) benzodifuran derivatives whose chemical structure is reported in Fig. 1.

In particular, the specific reaction conditions chosen resulted in the formation of the **BF** derivative in prevalent amount as compared to **BDF** counterpart, opposite to what obtained by Obushak [32]. A careful chemical-physical characterization was performed on all the isolated compounds. The chemical identity of the compounds was confirmed by NMR analysis. Phase behavior was investigated by means of a differential scanning calorimetry (DSC) analysis. Their thermal stability was evaluated by thermogravimetric analysis (TGA). The optical properties of the compounds were assessed by UV–Vis spectroscopy in tetrahydrofuran (THF) solution. An investigation on the potential biological activity of the reported compounds was performed by analyzing their antiproliferative effect on prostatic tumour cells (PC-3) and some nucleic acid binding activities. Finally, a mechanistic study, performed by means of CD and fluorescence techniques, was carried out on the most promising molecule, **BF1**, with the aim of relating its antiproliferative properties to the ability to bind telomeric DNA (proven by CD and fluorescence techniques on tel_{22} G4 DNA), and highlighting its unexpected impact on cell cycle progression.

2. Materials and methods

2.1. Chemical-physical characterization

^{1}H and ^{13}C NMR spectra were recorded with a Varian Inova 500-MHz apparatus. The thermal behavior of the compounds was studied by differential scanning calorimetry (Perkin-Elmer Pyris 1, nitrogen atmosphere, scanning rate 10 K/min) and thermo-gravimetric analysis (TGA 4000, air, 10 K/min). UV/Vis absorption spectra of the prepared compounds in THF solution, were recorded with a Jasco V560 spectrophotometer at 200 nm/s scan rate.

2.2. Synthesis

All the intermediates used in the synthetic procedures described below, have been purchased by Sigma Aldrich and Acros Organics, and used without further purification. The purity of all final synthetic compounds (**BF1**, **BF2**, **BDF1** and **BDF2**) was ≥95%.

2.2.1. 4′-Nitro-[1,1′-biphenyl]-2,5-dione (*NO2BQ*)

4-Nitroaniline (13.0 g, 0.0941 mol) was suspended in 30 mL of water and kept under stirring in an ice/water bath. 24 mL of HCl 37% were added to the system. Then, a solution of $NaNO_2$ (7.00 g, 0.101 mol) in 25 mL of water was added dropwise during five minutes while the temperature was maintained below 4 °C. After 30 min the obtained solution containing the diazonium salt was poured, dropwise, in 1000 mL of a solution of sodium acetate (50 g) and *p*-benzoquinone (13.0 g, 0.120 mol). A strong effervescence was produced along with the formation of a

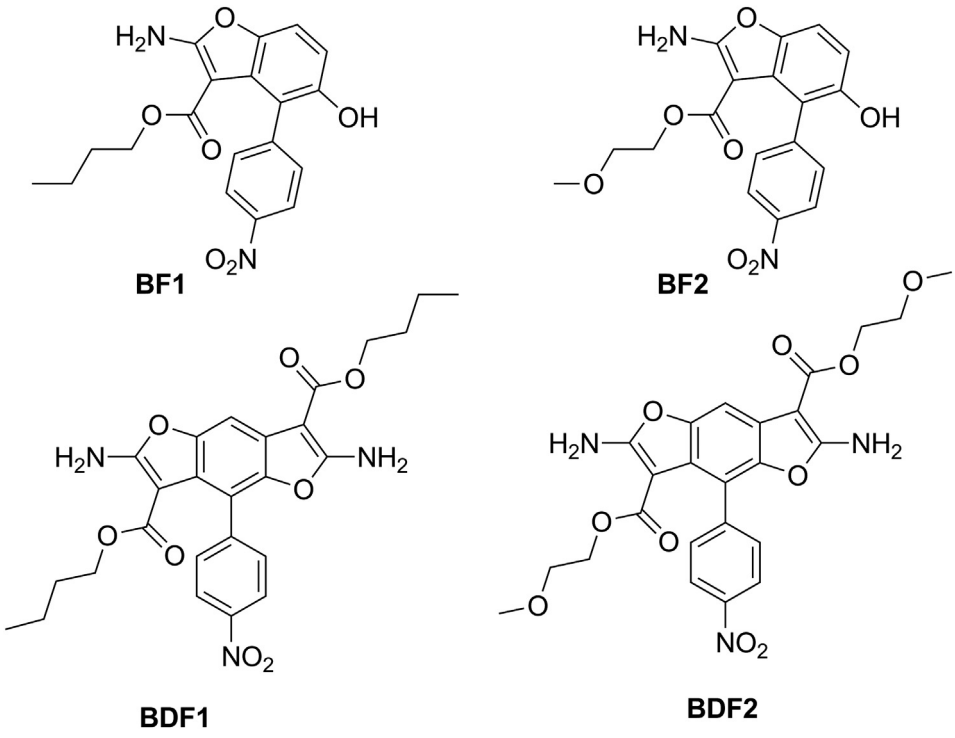

Fig. 1. Benzofuran (**BF**) and benzodifuran (**BDF**) derivatives prepared in this paper.

yellow-brown precipitate that was recovered by means of suction filtration. The recovered product was kept under stirring in ethanol over 30 min and refiltered. The filtrate was then washed in warm water (≈50 °C) and refiltered. 20.4 g of a yellow-greenish solid were recovered which was used in the next reaction step without further purification. Yield was 94%.

M.p.: 130 °C

^{1}H NMR ($CDCl_3$, 500 MHz): δ (ppm) 6,86–6.90 (m, 3H); 7,61 (d,2H, J = 9.0 Hz); 8,26 (d, 2H, J = 9,0 Hz).

*2.2.2. Synthesis of dibutyl 2,6-diamino-4-(4-nitrophenyl)benzo[1,2-b:4,5-b′]difuran-3,7-dicarboxylate (**BDF1**) and butyl 2-amino-5-hydroxy-4-(4-nitrophenyl)benzofuran-3-carboxylate (**BF1**)*

2.00 g of **NO2BQ** (8.73 mmol) and 2.464 g of butyl-cyanoacetate (17.5 mmol) were suspended in 7 mL of methanol. 2.6 mL of $NH_{3(aq)}$ 30% were added during 30 s: the color of the suspension turned immediately to blue-green and, after few seconds, to brown. The system was kept under stirring over 30 min and then placed at −32 °C in a freezer overnight. The precipitate was then recovered by means of suction filtration, washed with 10 mL of cold ethanol and refiltered. 0.489 g of a yellow-greenish solid was obtained corresponding to **BDF1** (yield 11.1%). The filtrated ethanol solution was poured dropwise in 120 mL containing 0.5 g of $CaCl_2$ and cooled at 0 °C by an external ice/water bath. A yellow precipitate formed that was collected by suction filtration. This yellow solid corresponded to **BF1** and amounted to 1.248 g (yield 38.0%).

BDF1 data:

M.p.: 240,1 °C

^{1}H NMR (DMSO-d_6, 400 MHz): δ (ppm) 0.72 (t, 3H, J = 7.0 Hz); 0.97–1.01 (m, 7H); 1.45 (m, 2H); 1.72 (m, 2H); 3.58 (t, 2H, J = 6.4 Hz); 4.24 (t, 2H, J = 6.4 Hz); 7.41 (s, 1H); 7,63 (s, 2H); 7.67 (d, 2H, J = 8.8 Hz); 7,78 (s, 2H); 8.29 (d, 2H, J = 8.8 Hz).

^{13}C NMR (DMSO-d_6, 100 MHz): δ (ppm) 13.84; 14.08; 18.86; 19.36; 30.37; 30.99; 62.49; 62.97; 82.28; 82.46; 100.07; 113.63; 118.63; 121.77; 122.90; 131.58; 143.74; 146.57; 146.85; 164.35; 164.81; 165.46; 166.62.

CHN elemental analysis: Found: C 61.06 H 5.25 N 8.10%; Molecular Formula $C_{26}H_{27}N_3O_8$ requires: C 61.29; H 5.34; N 8.25%.

BF1 data:

M.p.: 218,7 °C.

^{1}H NMR (DMSO-d_6, 500 MHz): δ (ppm) 0.67 (t, 3H, J = 7.0 Hz); 0.99 (m, 4H); 3.46 (t, 2H, J = 6.0 Hz); 6.60 (d, 1H, J = 8,5 Hz); 7.15 (d, 1H, J = 8.5 Hz); 7.45 (d, 2H, J = 7.0 Hz); 7.70 (s, 2H); 8.15 (d, 2H, J = 7.0 Hz); 9.15 (s, 1H).

^{13}C NMR (DMSO-d_6, 125 MHz): δ (ppm) 13.82; 18.86; 30.37; 62.48; 82.84; 108.66; 110.33; 117.26; 122.42; 125.77; 131.89; 142.74; 146.03; 146.78; 151.51; 164.51; 167.22.

CHN elemental analysis: Found: C 61.90 H 4.80 N 7.66%; Molecular Formula $C_{19}H_{18}N_2O_6$ requires: C 61.62; H 4.90; N 7.56%.

2.2.3. Synthesis of 7-(2-methoxyethyl) 3-(methoxyethyl) 2,6-diamino-4-(4-nitrophenyl)benzo[1,2-b:4,5-b′]difuran-3,7-dicarboxylate (BDF2) and methoxyethyl 2-amino-5-hydroxy-4-(4-nitrophenyl)benzofuran-3-carboxylate (BF2)

2.00 g of **NO2BQ** (8.73 mmol) and 1.374 g of methoxyethyl-cyanoacetate (9.60 mmol) were suspended in 7 mL of methanol. 2.6 mL of $NH_{3(aq)}$ 30% were added during 30 s: the color of the suspension turned immediately to blue-green and, after few seconds, to brown. The system was kept under stirring over 30 min and then placed at −32 °C in a freezer overnight. The precipitate was then recovered by means of suction filtration, washed with 10 mL of cold ethanol and refiltered. 0.269 g of a red-brown solid was obtained corresponding to BDF2 (yield 6.1%). The filtrated ethanol solution was poured dropwise in 120 ml containing 0.5 g of $CaCl_2$ and cooled to 0 °C by an external ice/water bath. A yellow precipitate formed that was collected by suction filtration. This yellow solid corresponded to BF2 and amounted to 0.818 g (yield 25.4%).

BDF2 data:

M.p.: 233,5 °C.

^{1}H NMR (DMSO-d_6, 400 MHz): δ (ppm) 3.07 (t, 2H, J = 4.8 Hz); 3.11 (s, 3H); 3.34 (s, 3H); 3.70 (t, 2H, J = 4.8 Hz); 3.75 (t, 2H, J = 4.8 Hz); 4.35 (t, 2H, J = 4.8 Hz); 7.45 (s, 1H); 7.65–7.67 (m, 4H); 7,77 (s, 2H); 8.28 (d, 2H, J = 8.8 Hz).

^{13}C NMR (DMSO-d_6, 125 MHz): δ (ppm) 58.21; 58.52; 58.53; 61.53; 62.21; 69.84; 70.62; 82.20; 82.45; 100.23; 113.62; 118.79; 122.89; 131.54; 143.50; 143.74; 146.66; 146.80; 163.74; 164.52; 165.50; 166.53.

CHN elemental analysis: Found: C 56.10 H 4.40 N 8.05%; Molecular Formula $C_{24}H_{23}N_3O_{10}$ requires: C 56.14; H 4.52; N 8.18%.

BF2 data:

M.p.: 182,9 °C.

^{1}H NMR (DMSO-d_6, 500 MHz): δ (ppm) 3.05 (t, 2H, J = 4.5 Hz); 3.10 (s, 3H); 3.69 (t, 2H, J = 4.5 Hz); 6.65 (d, 1H, J = 8.5 Hz); 7.19 (d, 1H, J = 8.5 Hz); 7.48 (d, 2H, J = 7.0 Hz); 7.73 (s, 2H); 8.19 (d, 2H, J = 7.0 Hz); 9.20 (s, 1H).

^{13}C NMR (DMSO-d_6, 125 MHz): δ (ppm) 58.24; 61.55; 69.83; 82.84; 82.84; 108.79; 110.37; 117.30; 122.45; 125.94; 131.89; 142.85; 146.03; 146.60; 151.53; 163.99; 167.14.

CHN elemental analysis: Found: C 57.70 H 4.27 N 7.52%; Molecular Formula $C_{18}H_{16}N_2O_7$ requires: C 57.70; H 4.33; N 7.40%.

2.3. Cell culture

Human prostate cancer PC-3 cells were maintained in RPMI 1640 medium (GIBCO, USA) while human cervix epithelioid carcinoma (Hela), human osteosarcoma cells (U2OS) and human breast carcinoma cells (MCF-7) were maintained in DMEM medium (GIBCO, USA). Both media were supplemented with 10% fetal bovine serum (GIBCO, USA), 2 mM L-glutamine (LONZA, Belgium) at 37 °C, in a 5% CO_2 humidified atmosphere and harvested at approximately 90% confluence. Normal human dermal fibroblasts (NHDF) within 8th passage were cultured in fibroblast growth medium (FGM-2; Lonza, Milan, Italy) containing 2% FBS, 50 μg/mL gentamycin and amphotericin B, 10 μg/mL fibroblast growth factor and insulin.

2.4. Cell-based assays

Cell viability was assessed by Cell counting Kit 8 (CCK-8) assay. Briefly, 4×10^3 cancer cells were seeded in 50 μL medium per well in 96-well flat-bottom microplates and incubated overnight to allow cell adhesion. Subsequently, culture medium was removed, and cells were incubated with different concentrations of compounds, appropriately diluted with dimethylsulfoxide (DMSO) (Sigma-Aldrich), in quadruplicate for 24 h. Then, 10 μL of the CCK-8 solution were added to each well and the plate was incubated for 1 h at 37 °C, in a 5% CO_2 humidified atmosphere. Finally, absorbance was measured at 450 nm using a microplate reader (Multiskan Fc 10,094, Thermo). The relative number of viable cells was expressed as optical density (O.D.).

Crystal violet assay was performed to determine IC_{50} value. Shortly, culture medium was removed, cells were washed with Phosphate-Buffered Saline (PBS), fixed and stained with 0,1% (w/v) crystal violet in 25% methanol (Sigma-Aldrich); after 30 min cells were washed twice with double distilled water and let dry. Then, crystal violet was dissolved in 10% acetic acid solution and absorbance was measured at 595 nm using a microplate reader. The IC_{50} value was calculated according to the GraphPad Prism 5 software. All data were expressed as mean ± SD. The experiment was performed three times.

2.5. Western blotting analyses

Following compound or control treatments, cells were washed three times with ice-cold PBS and collected at 4 °C in RIPA lysis buffer (Sigma-

Aldrich) added with complete protease inhibitors (Roche). Lysates were centrifuged at 13,000 rpm for 30 min at 4 °C. The protein concentration was determined in supernatants by the Bradford assay method.

For Western blotting analyses, protein aliquots (20 μg/lane) were run on SDS-PAGE (4–12% Life Technology) and then blotted onto PVDF membranes (Novex, Life Technology). Membranes were next incubated using as primary antibodies: anti-cyclin B1, anti-cyclin A2, anti-cyclin D1, anti-p21 $^{WAF1/Cip1}$ (Cell Signaling Technology); anti-caspase 3, anti-p16^{INK4a} (Santa Cruz Biotechnology); anti-PARP (Abcam); anti-vinculin (Biorbyt) and anti-GAPDH (Fitzgerald). PVDF membranes were finally incubated with the appropriate dilution of secondary antibodies (1 h at room temperature). Immunocomplexes were visualized by enhanced chemiluminescence and autoradiography according to the manufacturer protocol (Santa Cruz Biotechnology) and quantified by densitometric analysis with Image J software, using GAPDH (Glyceraldehyde 3-phosphate dehydrogenase) and Vinculin levels as a loading control.

2.6. Lactate dehydrogenase assay

The level of extracellular lactate dehydrogenase (LDH) released from damaged cells was measured as an indicator of cytotoxicity. Cells (4×10^3/well) were seeded in complete medium and treated with10 and 50 μM **BF1** for 24 h. Positive control was also included by treating cells with 0.01% Triton × 100. Untreated cells were used as negative control. Lysates and supernatant aliquots were then incubated with reaction buffer (0.7 mM *p*-iodonitrotetrazolium violet, 50 mM L-lactic acid, 0.3 mM phenazine methosulphate, 0.4 mM NAD, 0.2 M Tris/HCl pH 8.0) for 30 min at 37 °C. Absorbance was read at 490 nm in a microplate reader (Thermo, Multiskan Fc). The percent of LDH released was calculated as absorbance in the medium of treated cells divided by absorbance in the medium of treated cells plus absorbance in the total pellet of treated cells.

2.7. FACS analysis

Cell cycle was analyzed by FACS analysis. 5×10^5 PC-3 cells were treated with 10 and 50 μM **BF1** for 24 h. Subsequently, 5×10^5/mL cells were harvested, washed with PBS, centrifuged at 1400 rpm for 5 min and fixed with 95% ethanol. Then cells were stained with 50 μg/mL Propidium iodide (Sigma-Aldrich) for 30 min at dark and subjected to FACS analysis on a FACSCalibur flow cytometer (Becton Dickinson, BD), FL2 channel; $\lambda_{ex} = 488$ nm; $\lambda_{em} = 600$ nm. Data were analyzed using CellQuest and ModFit LT software.

2.8. CD binding studies

Circular dichroism (CD) spectra were registered on a Jasco J-715 spectropolarimeter equipped with a Peltier PTC-423S/15 in a dual-chamber Hellma (2 × 0.4375 cm) quartz cell or a quartz cell with a light path of 1 cm. All the spectra were averaged over 3 scans. The concentration of tel_{22} was 2.5 μM, while the benzofuran stock solutions were 80 mM in DMSO. CD denaturation experiments on tel_{22}/benzofuran complexes were realized recording the ellipticity at 295 with a temperature scan rate of 1 °C/min in the range 20–80 °C.

2.9. Fluorescence binding analysis

The data were acquired at 25.0 °C, using an excitation wavelength of 260.0 nm and a fluorescence emission wavelength ranging from 305 to 500 nm, using a Jasco FP 8300 spectrofluorometer and a cell of 10 mm path-length quartz cuvette. The acquisition parameters were set as follows: excitation and emission slits at 5 nm; 200 nm/min scan rate; 0.5 nm data interval averaging time at 0.050 s, PMT voltage at "medium". The fluorescence values recorded at 380 nm were extracted and transformed to $-\Delta_{fluorescence}$ which was obtained by subtracting them to the emission fluorescence intensity of the ligand-free oligo, and, then, plotted against **BF1** and **BDF1** concentrations. tel_{22} was used at the concentration of 50 μM in PBS 1× and incubated in the presence of increasing concentrations of **BF1** ranging from 0 to 100 μM and **BDF1** from 0 to 250 μM. A control assay was carried out employing as titrant the buffer of ligand to assess that both the dilution effect and DMSO addition (7, 3% v/v, for **BDF1** and **BF1** respectively) were under 3%, not affecting the results.

3. Results and discussion

3.1. Synthesis

The synthetic route for the synthesis of the novel benzofuran/benzodifuran derivatives here discussed is shown in Scheme 1.

NO2BQ was prepared according to a reported procedure [33] consisting in the diazotization of 4-nitroaniline and a carbon-carbon coupling of the obtained diazonium derivative on benzoquinone with release of molecular nitrogen. The substituted benzoquinone was then reacted with two different cyanoacetate esters in a basic environment in the previously discussed Craven reaction. In a recent work, Obushak et al. reported that this reaction leads typically to the formation of [1,2-b;4,5-b′]benzodifuran derivatives, either when an unsubstituted benzoquinone is used as starting compound and also when the reaction is carried on a wide range of substituted benzoquinones. In that work, anyway, Obushak showed that, by reacting **NO2BQ** with ethyl cyanoacetate, it was possible to isolate, beyond the expected benzodifuran derivative, a significative and characterizable amount of benzofuran derivative. In this paper, we used the same benzoquinone derivative, **NO2BQ**, and reacted it in the first place, with butyl cyanoacetate to observe the influence of the length of the alkyl chain of the ester on addressing the reaction towards the formation of the benzofuran (**BF1**) or benzodifuran (**BDF1**) derivative. What we observed is that, under the reaction conditions we set up, in our case the formation of **BF1** is always favoured over the formation of **BDF1**. In Fig. 2 we reported the possible reaction mechanism of Craven reaction, sketched on the basis of what previously proposed by Obushak.

The mechanism involved several stages and starts with the attack of the carbanion of the cyanoacetic esters on position 3 of **NO2BQ**, activated towards nucleophilic substitution by the combined action of a carbonyl and a 4-nitrophenyl group in *o*-position and the formation of the substituted hydroquinone ***a***. Intermediate ***a*** can undergo a intramolecular cyclization affording benzofuran derivative **BF** or be oxidized by the starting benzoquinone molecule to quinone ***b***. Then, ***b*** is attacked by a further molecule of cyanoacetic ester (***c***) and, after a double intramolecular cyclization, the benzodifuran derivative **BDF** is obtained. The relative speed of the first intramolecular cyclization (formation of **BF**) and oxidation reaction (formation of ***b***) determines the rate of **BF**/**BDF** amounts in the final product. In our case, the higher oxidative stability of **NO2BQ**, consequence of the high electron affinity of nitrophenyl group, could be considered responsible for the preferential formation of **BF**. As compared with the results obtained by Obushak, which reported the formation of **BF** and **BDF** derivative in yield of, respectively, 9 and 31%, our experimental results show the opposite behavior: regardless the feeding butyl cyanoacetate/**NO2BQ** ratio, varying from 1 to 3, a preferential formation of **BF1** is observed. The main difference in the reaction conditions used by us and Obushak is that we worked in a highly concentrated reaction medium and used a worse solvent, methanol instead of ethanol. Different reaction conditions were tried, in particular by varying ester/quinone feeding ratio and solvent (ethanol or methanol). The better results were obtained by using a feeding ratio ester/quinone of 2, in methanol as solvent: in this case, the yield for the formation of **BF1** and **BDF1** was, respectively, of 38 and 11%. We established a work-up procedure extremely easy and based on the different solubility of **BF1** and **BDF1**: after the reaction time, the reaction system was placed in a freezer at −32 °C overnight; at this temperature

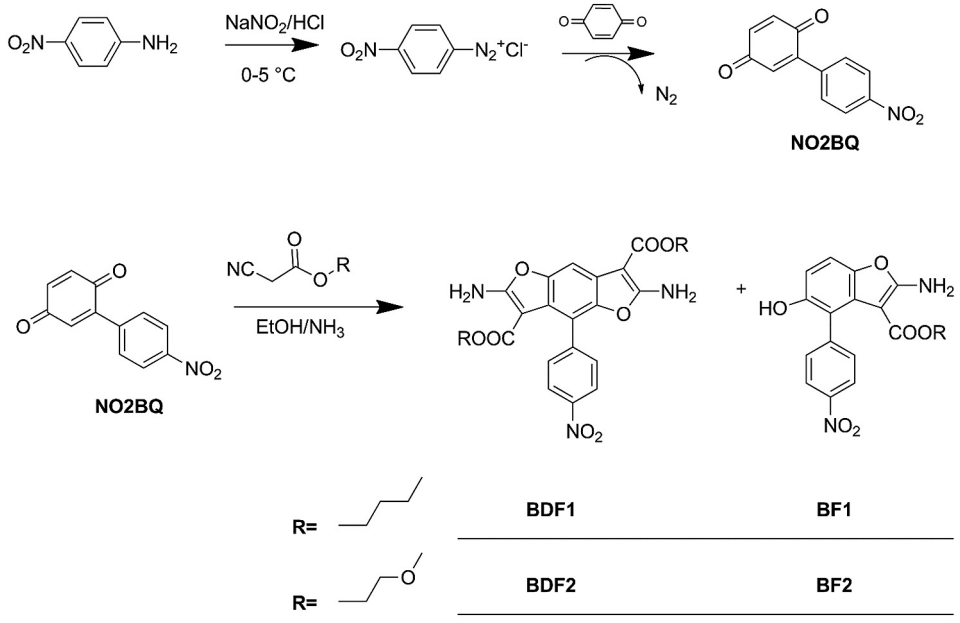

Scheme 1. Synthetic pathway for the preparation of **BF** and **BDF** derivatives discussed in this paper.

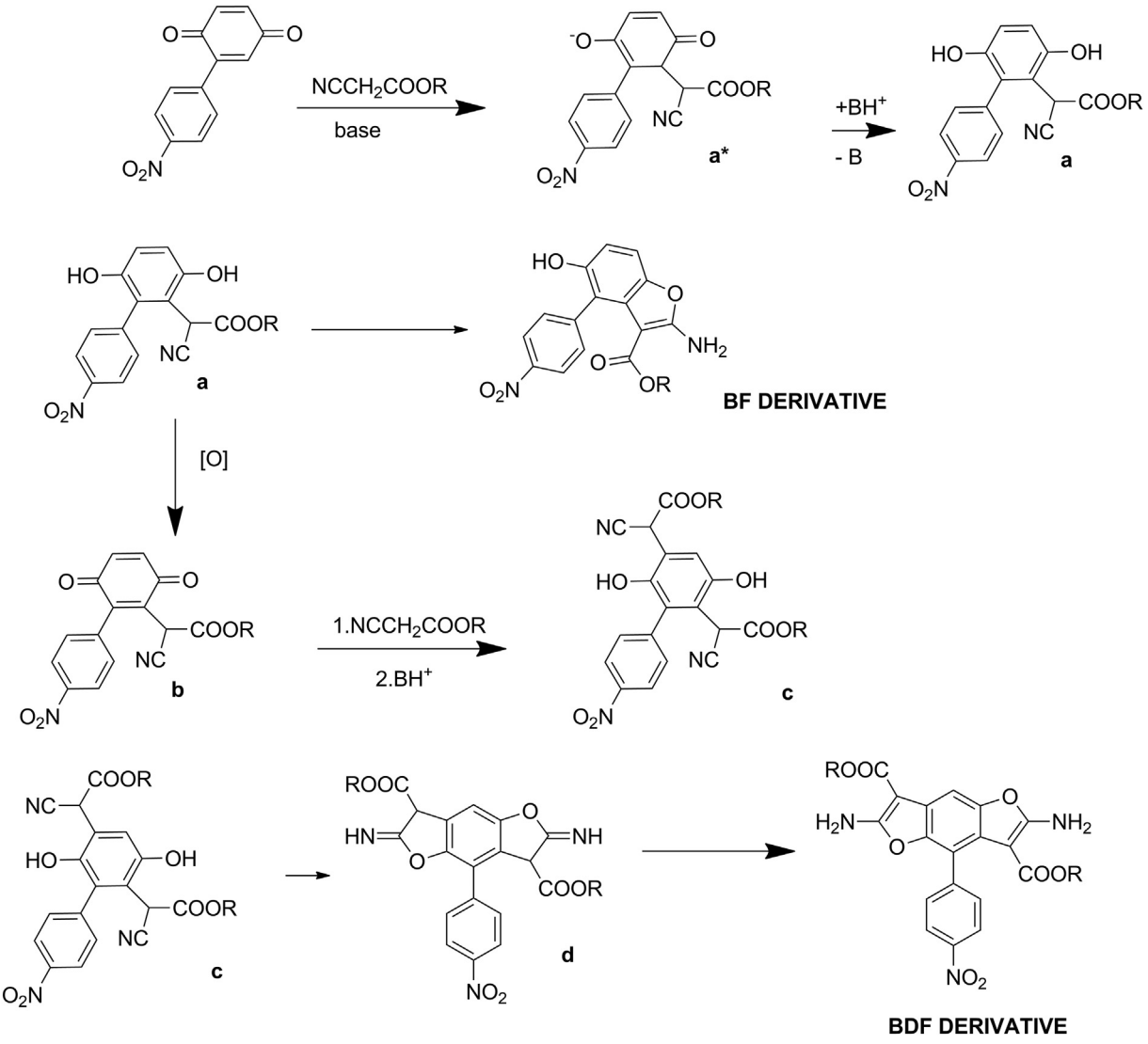

Fig. 2. Reaction mechanism of Craven reaction.

both **BF1** and **BDF1** are scarcely soluble and precipitate. Once the raw precipitate is recovered by suction filtration, it is washed in ethanol at room temperature: **BDF1** is insoluble in ethanol and is recovered by filtration, **BF1** is soluble in ethanol and is recovered by precipitating the mother liquors of the previous filtration in water. By using this procedure, the two compounds were recovered with high degree of purity. In the Supporting Information we report in Table S1 the different reaction conditions used and the resulting yields for the obtainment of the two compounds. The reaction was also performed by reacting **NO2BQ** with 2-methoxyethyl cyanoacetate to obtain products with side chains of similar length with respect to the previous one but with higher flexibility and better affinity to water. Different esters/quinone ratios were used also in this case and the better results were obtained when this ratio was set equal to 1.1 as shown in Table S2 in the Supporting Information: yield of **BF2** and **BDF2** were, respectively, 25.4 and 6.1%. By increasing the relative amount of ester, while the yield in **BDF2** did not vary significantly, only traces of the benzofuran derivative (**BF2**) were recovered: we assumed that the excess of ester played a solubilizing effect and did not allow the precipitation of the benzofuran derivative.

All the prepared compounds were characterized by NMR spectroscopy analysis and proton and carbon spectra are reported in the Supporting information (Figs. S1–S8). The inspection of the spectra of the two benzodifuran derivatives, **BDF1** and **BDF2**, reveals that the asymmetry of the molecules results in the splitting of the signals relative both to ester tails and the amino groups. The spectra of benzofuran derivatives are instead characterized by a resonance beyond 9 ppm, corresponding to phenolic proton and two doublets around 7 ppm, integrating each for one proton and associated to the aromatic protons of the starting benzoquinone ring. Solubility assays performed on all compounds confirmed that the ethyleneoxide chain derivatization conferred to benzofuran derivatives an increased water solubility, as expected, and a lower solubility in apolar solvent (Table S3, Fig. S9 and S10).

3.2. Thermal analysis

The phase behavior of all the synthesized compounds was investigated by means of DSC analysis and the relative thermograms are reported in Fig. 3.

They are all characterized by sharp endothermic peaks, corresponding to the melting of compounds, confirming their high purity degree. Benzodifuran derivatives **BDF1** and **BDF2** present a melting point of 240 and 234 °C, respectively. The latter is moreover characterized by a polymorphic behavior: at around 180 °C it is, in fact, observable the melting of a metastable crystalline phase and the subsequent crystallization (exothermic peak) in the thermodynamically stable crystalline phase. This polymorphic behavior could be related to the flexible nature of the two ethyleneoxide chains that can give rise to different conformations and drive different crystal packing. As expected, the benzofuran derivatives show lower melting points, of 221 and 184 °C respectively, for **BF1** and **BF2**.

Thermal stability of the compounds was investigated by TGA analysis and the thermograms are presented in Fig. 4. The decomposition temperature of all the compounds, determined as the temperature corresponding to a weight loss of 5%, is fair high; specifically, it is around 240 °C for **BF** derivatives and 260 °C for **BDF** analogous. Thermal

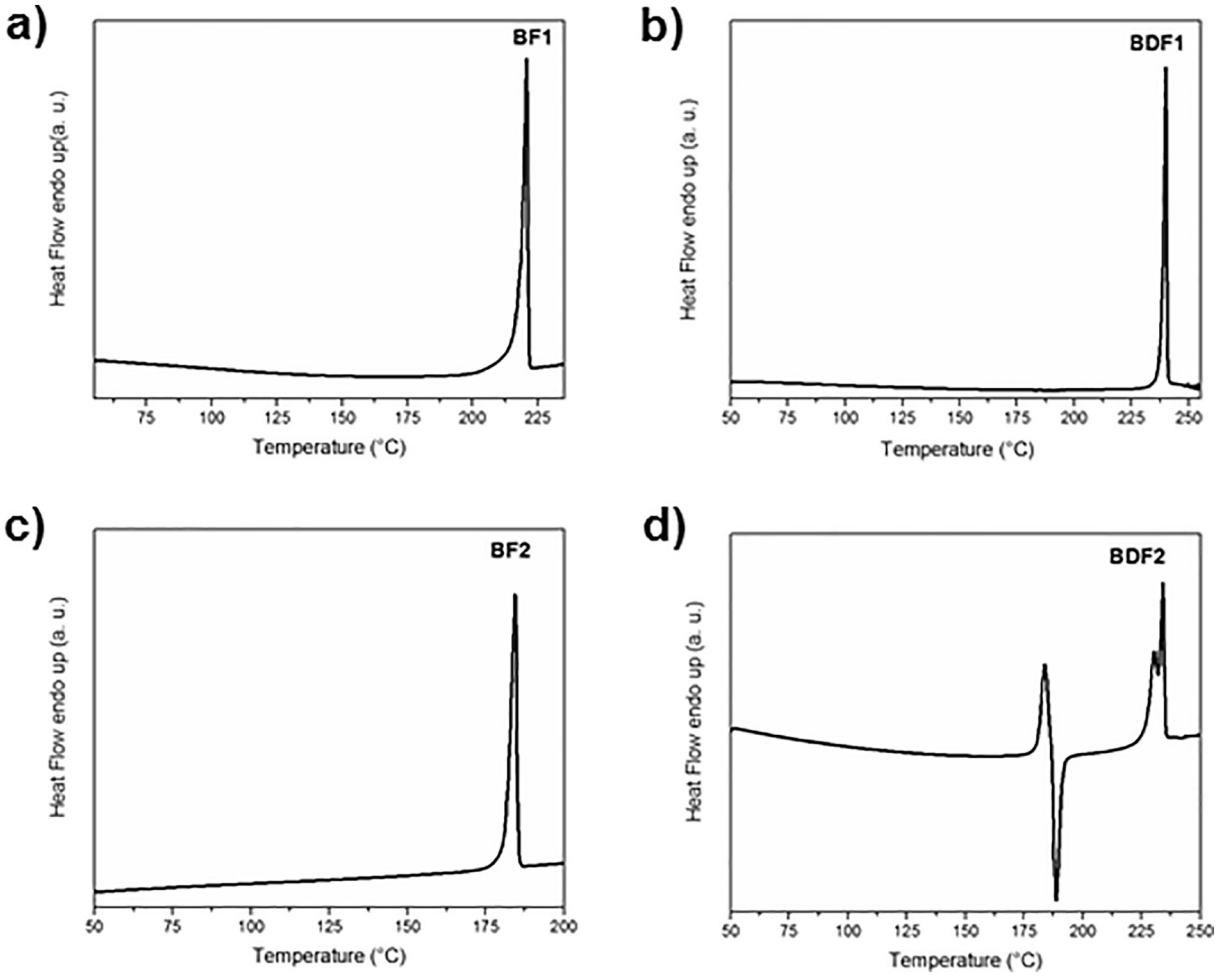

Fig. 3. DSC traces of the four synthesized compounds.

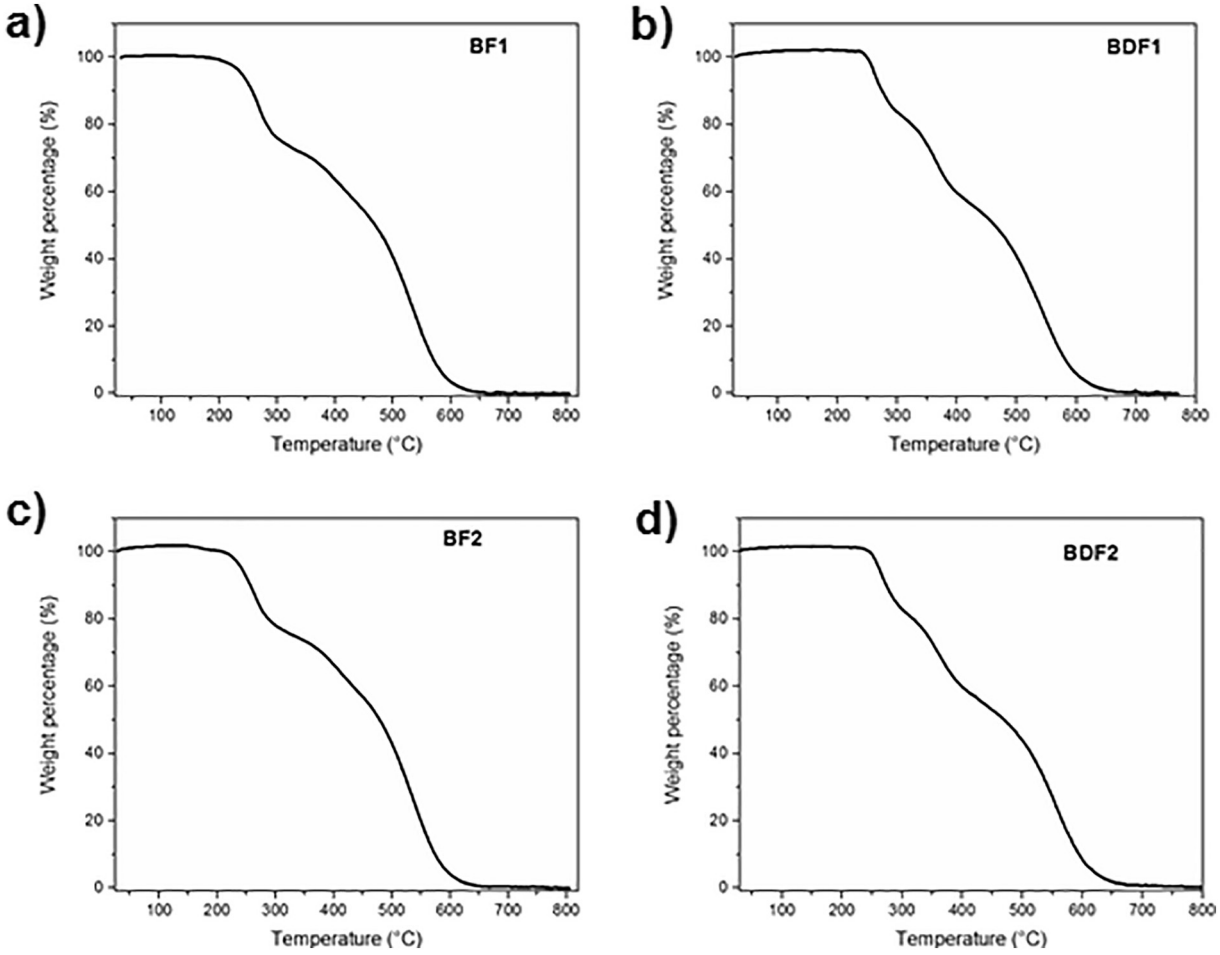

Fig. 4. Thermo-gravimetric analysis graphs of the prepared compounds.

properties of all compounds are summarized in Table 1. **BDF** compounds presented a similar TGA plot, characterized by three successive decomposition steps. In the first step (centred at around 270 °C) the observed weight decrease (≈20%) is consistent with the loss of one of the two ester tails: we could speculate that the alcohol group is removed first and successively a molecule of CO is lost with a possible cyclization involving the amino group. Indeed, a slight change of the slope is observable in this step. The second decomposition step, centred at around 350 °C has about the same entity of the first and can be associated to the loss of the second ester tail. Finally, the compounds show a gradual decomposition (centred at 530 °C) extending up to 650 °C. For what concerns the **BF** compounds, as expected, decomposition occurs only in two steps: the first, centred at around 260 °C, corresponds to a weight diminishment of ≈27% and is consistent with the loss of the ester tail. Then, the compounds undergo a second gradual decomposition step centred at 530 °C and extending up to 650 °C.

Table 1
Thermal properties of the synthesized compounds.

Compounds	T_m (°C)[a]	T_d (°C)[b]
BF1	220.5	239.2
BDF1	240.0	262.2
BF2	184.5	242.5
BDF2	234.2	261.8

[a] Measured by DSC analysis run in nitrogen environment at 10 °C/min scan rate.
[b] Determined as the temperature corresponding to a weight loss of 5% during a TGA analysis performed in air atmosphere at 20 °C/min scan rate.

3.3. Optical analysis

The prepared compounds underwent optical analysis by UV–Vis spectrophotometry, performed in THF solution. Optical spectra are reported in Fig. S11. Qualitatively, **BF** derivatives showed two main optical features, the first at around 270 nm and the second, of lower intensity, at about 340 nm. **BDF** derivatives are instead characterized by a main absorption band at around 280 nm, showing a vibronic structure, and a second band, broader and with lower intensity, in the visible region of the spectrum, at about 415 nm. **BDF** derivatives show an overall red shifted absorption behavior as compared to the corresponding benzofuran systems. Optical properties of the compounds are reported in Table S4. From a quantitative point of view, all molecules are good absorbers in the UV zone of the spectrum with molar extinction coefficients ranging from 20,000 to 25,000 for **BF** and **BDF** series, respectively.

3.4. *BF1* treatment decreases PC-3 cell viability

In order to evaluate the anticancer potential of the two families of aromatic compounds, the survival of human PC-3 cells was determined by CCK-8 assay after exposure to increasing doses of the benzofuran derivatives or vehicle control (DMSO) for 24 h. In particular, **BF1** induced a loss of viability in a dose dependent manner with an IC_{50} value of 33 μM as shown in Fig. 5 and Table 2. The other compounds presented less significant cytotoxic effects, with **BDF1** being the most effective in the benzodifuran family but still less active than benzofurans. These data suggest higher anticancer efficacies associated to more hydrophobic members of both classes, however an increased activity can be

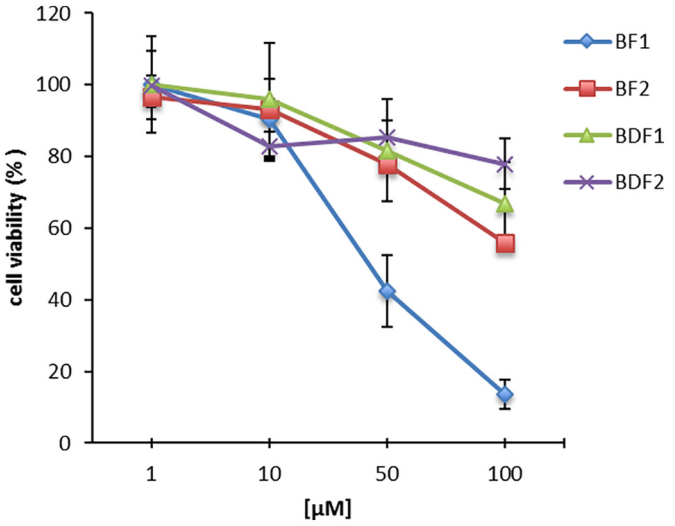

Fig. 5. Effect of benzofuran derivatives on PC-3 cell viability; PC-3 cells (4×10^3) were seeded in 96-well plates and treated with different concentrations of benzofuran derivatives for 24 h. DMSO treated cells were used as vehicle control. After treatment CCK-8 assay was performed. Data are shown as percentage of control ($n = 3$, ± SD).

correlated to the reduction of the number of fused cycles, passing from benzodifuran to benzofuran derivatives.

Since **BF1** exhibited higher toxicity compared to the other derivatives, its effect was investigated against a panel of human cancer cell lines to ascertain whether its activity was dependent on cancer type or not. As shown in Table 3, in the case of HeLa, U2OS and MCF-7 we observed IC_{50} values comprised between 48 and 76 μM, which are significantly higher than that found for PC-3 cells. Interestingly, other literature benzofuran compounds have shown important anticancer potential, with a 3-acyl-5-hydroxybenzofuran synthesized by Li et al. [34] exhibiting a remarkable antiproliferative activity against human breast cancer (MCF-7) cells with a IC_{50} of 43 μM, comparable to that found for **BF1** on the same cell lines.

As control, similar experiments were carried out under the same experimental conditions on normal human fibroblasts. Interestingly, at a 50 μM concentration, **BF1** induces a toxicity lower (ca. 57%) than that observed on PC-3 cells (Fig. 6) suggesting, thus, that this compound could exert its cytotoxic activity preferentially on cancer cells.

3.5. *BF1* induces S phase arrest during cell cycle progression

To investigate the molecular mechanism underpinning the reduced cancer cell proliferation triggered by **BF1**, cytotoxicity and apoptosis biomarkers were investigated. LDH is a stable enzyme present in all cell types and the appearance of this protein in the extracellular milieu is a conventional marker for the loss of membrane integrity and the presence of necrosis [35]. The treatments with **BF1** over 24 h at 10 μM and 50 μM dosages had effects comparable to that seen on DMSO-exposed cells, indicating that the suppression of cell viability was not associated with necrotic process (Fig. 7A).

Since it is widely recognized that activation of executioner caspases is a major hallmark of apoptotic cell death [36], western blot analysis was performed on whole cell to assess whether **BF1** induced caspase 3 activation in PC-3 cells. This marker was absent in PC-3 cells treated with **BF1** but detected in samples from etoposide-treated Jurkat cells used as a positive control (Fig. 7B). Altogether, our results suggest that **BF1** does not suppress PC-3 cell viability via necrosis or apoptosis mechanisms.

Furthermore, we have explored the effect of **BF1** treatment in PC-3 cells on the expression of p21 and p16, classical markers of senescence upregulated in cancer cells [37,38]. No increase in p21 and p16 expression was detected after 24 and 72 h of treatment, suggesting that cancer cells do not enter senescence as effect of **BF1** (Fig. S12).

Thus, to better understand the mechanism of **BF1**-mediated proliferation inhibition, we proceeded to examine the effect of **BF1** on the cell cycle by FACS. Since, once treated with vehicle (DMSO) control, cells had cycle profiles similar to those treated with PBS (data not shown), DMSO was used as a control in the below-described experiments.

In these assays, while cell populations in the G0/G1 and S phases were about 35% of control cells, after 24 h incubation with **BF1** with different concentrations (at 10 μM and 50 μM) the S population was noticeably enhanced to 56% and 87%, respectively, whereas G0/G1 and G2/M populations were significant decreased (Fig. 8A). As well known, cell cycle progression is regulated by the sequential activation and inactivation of cyclin/cdk complexes [39]. In eukaryotic cells, on one hand, cyclin E/cdk2 complex leads to initiation of DNA replication, while cyclin B/cdk1 is implied in both entry into and progression through mitosis. On the other hand, cyclin A/cdk2 plays a role in progression through S phase, with a large pool also activated in G2 phase [40]. Thus, to identify cell-cycle regulators, we examined the expression of cyclins and cyclin-dependent kinases. PC-3 cells were treated with **BF1** over 24 h and cell lysates were prepared for Western blot analysis. As shown in Fig. 8B, the treatment with **BF1** 50 μM led to a

Table 2
Half maximal inhibitory concentration (IC_{50}) of the prepared compounds on PC-3 cells.

Compounds	IC_{50} [μM]
BF1	33 ± 0.4
BF2	142 ± 0.18
BDF1	146 ± 0.11
BDF2	>200

Data average of three independent experiments ± SD determined by crystal violet assay (24 h incubation time). Solutions of the investigated compounds were prepared by diluting a freshly prepared stock solution (10^{-2} M in DMSO) in culture medium.

Table 3
Growth inhibition of **BF1** on different cell lines.

Cell line	IC_{50} BF1 [μM]
MCF-7	76 ± 0.02
HeLa	48 ± 0.01
U2OS	56 ± 0.04

Data average of three independent experiments ± SD determined by crystal violet assay (24 h incubation time).

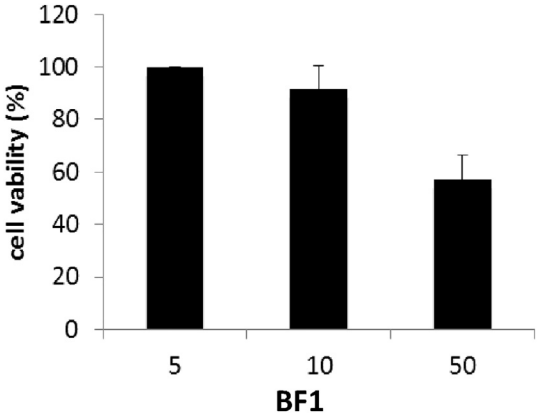

Fig. 6. Determination of the cytotoxic effect of **BF1** on NHDF. Cells were seeded at a density of 2×10^4 cells/cm^2 and treated with increasing amounts of **BF1** for 24 h. Cell viability was measured by CCK-8 assay, and values were expressed as percentage respect to controls (cells treated with increased amounts of DMSO). Each value expresses an average ± SD of two separate experiments performed in quadruplicate.

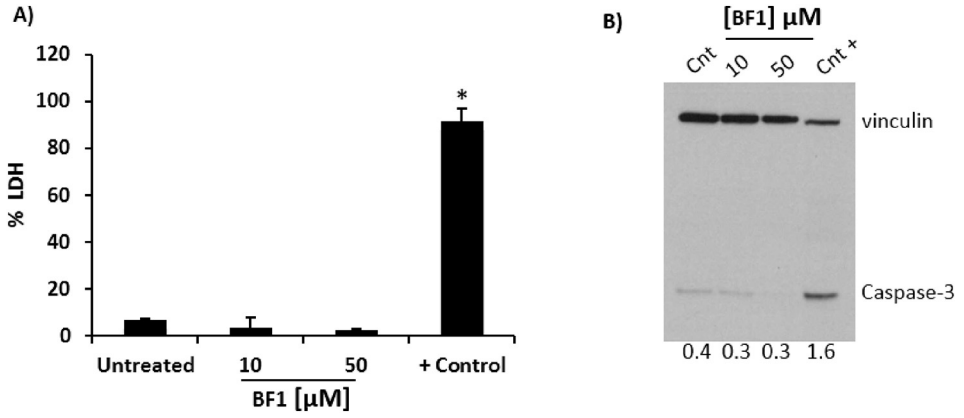

Fig. 7. BF1 does not induce necrosis or apoptosis in PC-3 cells. A) Cytotoxic effect of **BF1** at two different concentrations was evaluated by measuring the LDH release in the culture medium. PC-3 cells untreated or treated with 0.01% Triton × 100 were used as a control. Data are reported as percentage of maximum LDH release and values are presented ±SD of two independent experiments carried out in triplicate (*$P < 0.05$). B) Caspase 3 cleavage was assessed as a marker of apoptosis induction after treating cells with **BF1** at two different concentrations by Western blot. PC-3 cells treated with DMSO and Jurkat cells treated with 25 μM etoposide for 5 h were used as a negative and positive control respectively. Immunocomplexes were visualized by enhanced chemiluminescence and autoradiography and quantified by densitometric analysis with Image J software, using vinculin levels as a loading control.

downregulation of analyzed cyclins. Altogether, these results suggest that **BF1** treatment in prostatic cancer cells induces S phase arrest provoking also a downregulation of the analyzed cyclins and their normal regulation of cell cycle progression.

*3.6. Molecular mechanistic insight into **BF1** antiproliferative properties: quadruplex DNA binding*

It has been reported for heteroaromatic compounds with antiproliferative activity that their mode of action, independent of telomerase, is often associated to inhibition of cell cycle progression, in turn due to their ability to bind G-quadruplex structures [41]. Telomeric DNA, once structured in the G4 form, cannot be bound by telomerase inhibiting the telomere lengthening, notably responsible for cancer cell immortality. Thus, directing ligands to telomeric G4-structured DNA is a strategy to provoke anticancer effects interfering with telomerase activity [42]. These considerations prompted us to explore the interaction of **BF1**, with a model of the telomeric DNA, i.e. the G4-forming 22-mer sequence tel_{22}. CD spectroscopy was used to investigate the propensity of the mono-benzofuran derivative to interact with nucleic acids in analogy to previous reports. The same study was conducted also on the **BDF1** as a comparison. In order to investigate the influence of **BF1** and **BDF1** towards the G4 stability by a sequence taken from the human telomeric DNA, a 2.5 μM solution of tel_{22} G4

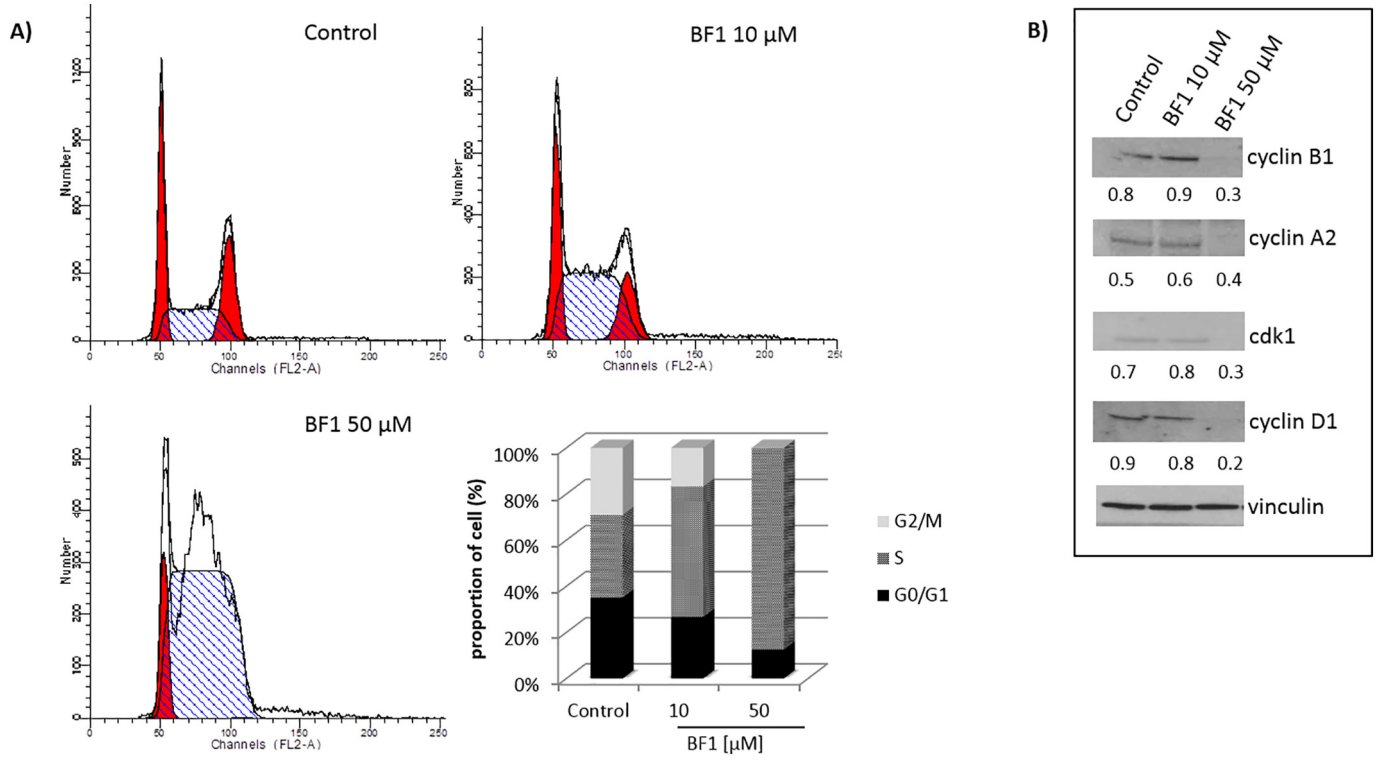

Fig. 8. Effect of BF1 on cell cycle cell progression in PC-3 cells. A) PC-3 cells were incubated at 37 °C with **BF1** (10 μM and 50 μM) for 24 h. Following incubation, cells were harvested, fixed and stained with propidium iodide and analyzed by flow cytometry. G0/G1, S and G2/M phases cell population percentage is represented in the histogram. The cells treated with DMSO were used as control. B) The expression of cell cycle regulating proteins was examined by Western blot. The blots were re-probed with anti-vinculin antibody for comparison of protein load. Densitometric analyses were obtained measuring optical density of bands normalized respect to the expression of vinculin, data after normalization are shown below the bands. The experiments were repeated three times and representative data are presented.

has been incubated with 30 equiv. of both compounds in phosphate buffer saline (PBS 1×: 137 mM NaCl, 2.7 mM KCl, 1.4 mM KH_2PO_4, 4.3 mM NaH_2PO_4, pH 7.4). The conformation adopted by tel_{22} G4 in PBS 1× prior to **BF1** and **BDF1** addition closely resembled that observed by Hudson et al. [43], as confirmed by comparison of CD spectra (Fig. 10 A and B). In particular tel_{22} in our experiments adopts mainly the basket-type topology corresponding to an antiparallel stranded intramolecular G4 consisting of three G-tetrads connected with three TTA loops (one being diagonal and other two lateral) [44].

In fact, CD exhibits positive CD bands near 240 and 295 nm and a negative one near 265 nm: these elements are typical of the above mentioned quadruplex structure [44]. CD profile of tel_{22} at 20 °C underwent a certain modification of the main positive band, and particularly at about 280 nm, when 30 equivalents of **BF1** were added to the G4 DNA solution as shown in Fig. 9A (left). The observed ellipticity increase can be explained in terms of slight modification of G4 topology from basket-type to a hybrid morphology, as an effect of the interaction with **BF1**, in analogy to the report of Ambrus et al. [44] In contrast, no variation was observed repeating the same experiment with **BDF1** (Fig. 9B right). Moreover, G4 stability has been analyzed by CD-melting experiments, monitoring the CD signal changes at 295 nm in the 20–80 °C temperature range; these analyses confirmed for the G4 a T_m of 60 °C as already found by Fuggetta et al. [45]. After incubation with both benzofuran derivatives, we repeated the CD denaturation (Fig. S13) demonstrating that **BF1** and **BDF1** do not affect the G4 thermal stability. Nevertheless, an effect of **BDF1** on CD properties of tel_{22} was detected at temperatures higher than 40 °C when our CD thermal denaturation of the **BDF1**/tel_{22} complex revealed an induced positive CD signal at about 325 nm. The same peak was observed also by Jain et al. [46] who studied 1,3-phenylene-bis (piperazinyl benzimidazole) derivatives as new quadruplex ligands. Similarly, we can hypothesize that above 40 °C **BDF1** interacts with the chiral environment of quadruplex grooves inducing a partial change in quadruplex conformation. Altogether, the above findings testify a molecular interaction of our tested compounds with telomeric DNA tract under consideration, with **BF1** being able to alter G4 conformation already at 20 °C and **BDF1** interacting with telomeric DNA only above 40 °C.

The interaction of tel_{22} G4 quadruplex with both benzofurans was analyzed also by intrinsic fluorescence of structured telomeric oligonucleotide as a function of ligand concentration [47].

Fluorescence emission at 380 nm showed a dose-response quenching upon the addition of the benzofurans (Fig. 10A and B), and the obtained Δ fluorescence intensities were plotted against the concentration values of **BDF1** and **BF1**, respectively as shown in Fig. 10C and D. Data were fitted with a 1:1 model of interaction, providing K_D values of 30 ± 2 and 150 ± 70 μM for **BF1** and **BDF1**, respectively [48,49]. In other words, fluorescence studies confirmed the ability of benzofuran derivatives to bind telomeric DNA and evidenced a greater affinity of **BF1** for tel_{22} with respect to **BDF1**.

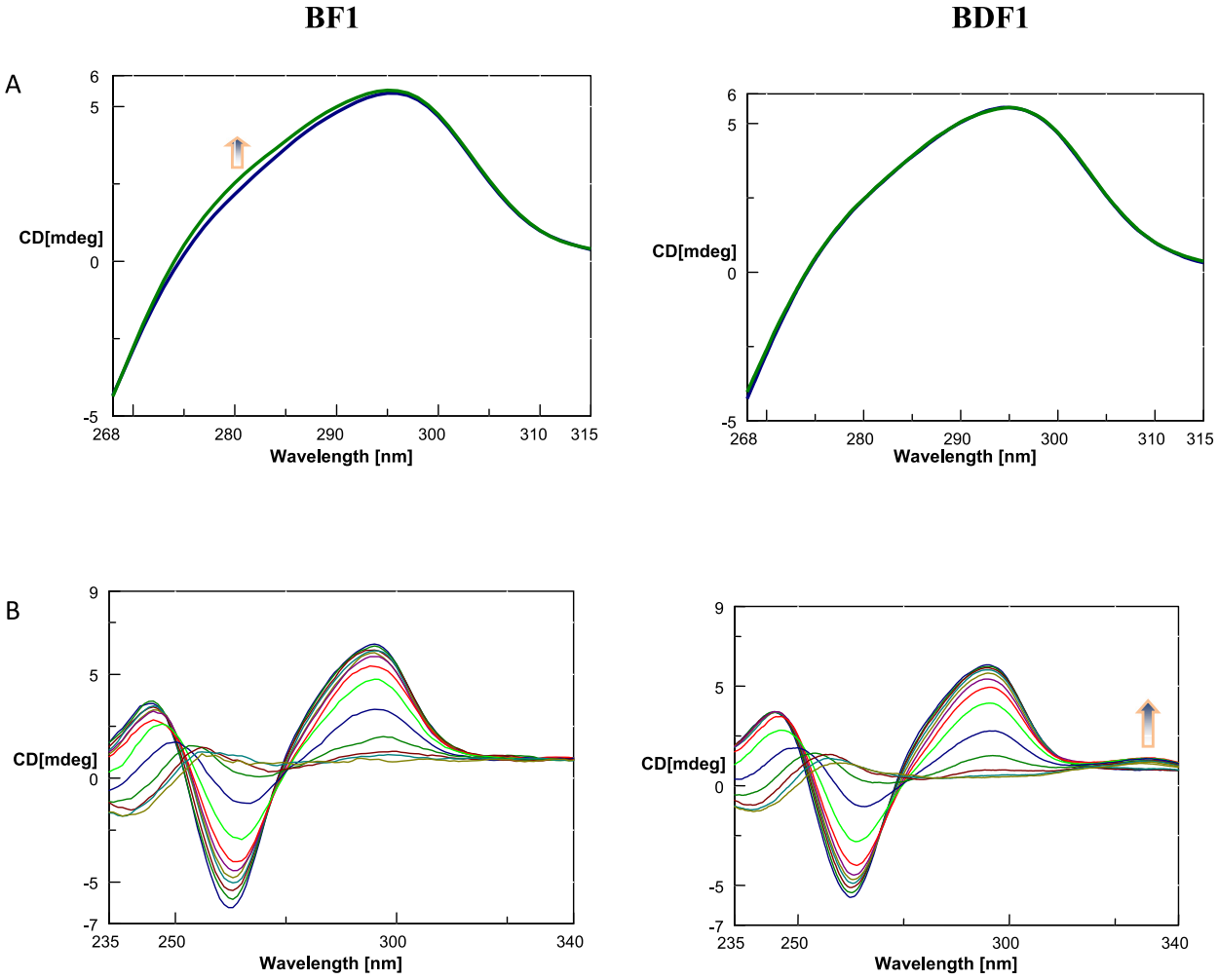

Fig. 9. A) CD spectra of 2.5 μM tel_{22} (blue line) in 1× PBS (T = 20 °C) and 2.5 μM tel_{22} + 30 equiv. of **BF1** (green line, left) or **BDF2** (green line, right). B) CD spectra at different temperatures (20–80 °C) of 2.5 μM tel_{22} + 30 equiv. **BF1** (left) and tel_{22} + 30 equiv. **BDF1** (right) in 1× PBS.

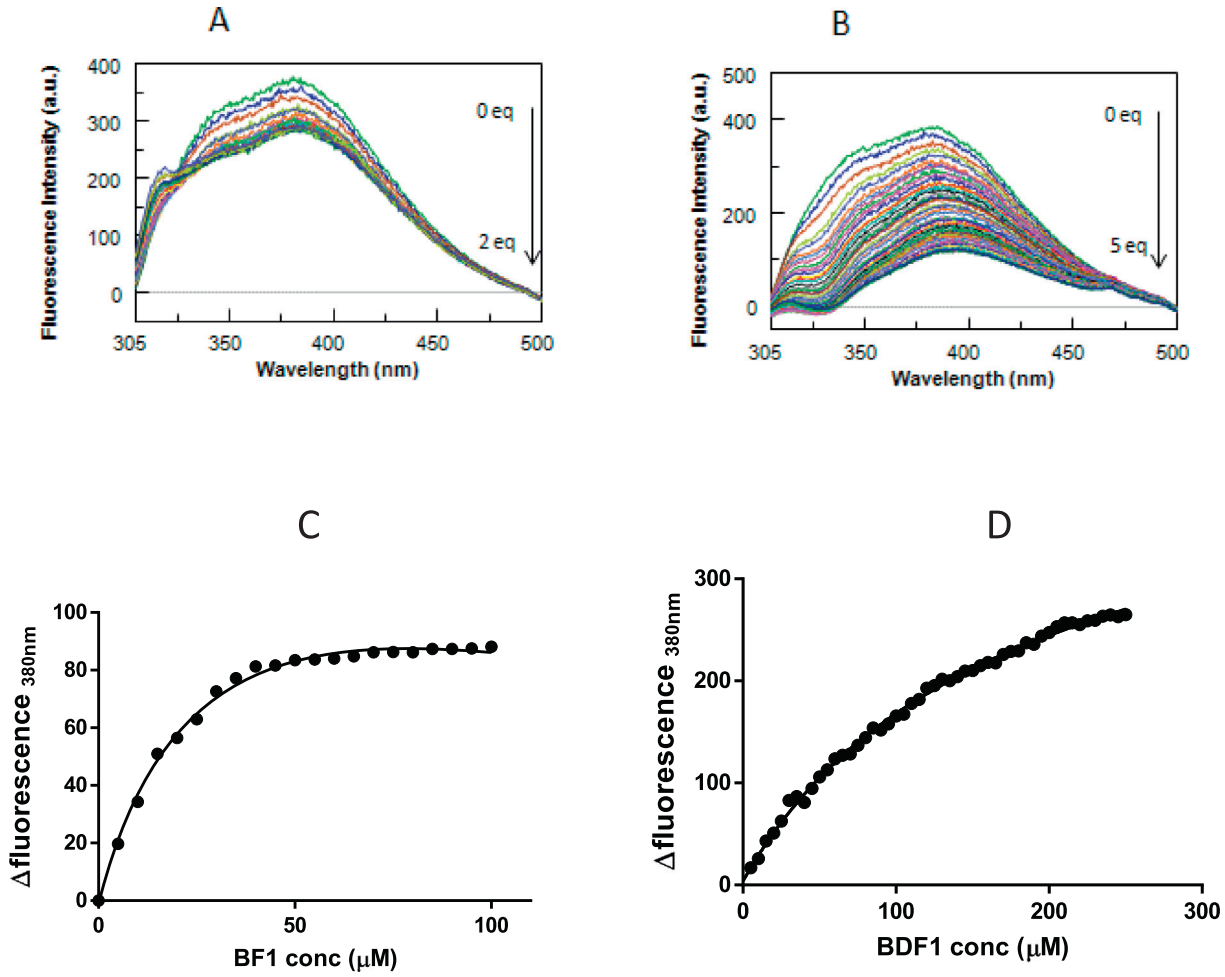

Fig. 10. BDF1 and **BF1** binding to tel_{22}: i) overlay of fluorescence spectra of tel_{22}-**BF1**(A) and tel_{22}-**BDF1**(B) (increasing amounts of equivalents of ligands are indicated by arrows); ii) intrinsic fluorescence quenching analysis showing the dose-response curve of the fluorescence values of tel_{22} G-4 at 380 nm plotted against the concentration values of (C) **BF1** and (D) **BDF1**.

4. Conclusion

In agreement with previous studies evidencing the nucleic acid-binding and antiproliferative activities of benzodifuran derivatives on human cancer cells, the present work has confirmed that also their 4-nitrophenyl variants are able to exert cytotoxic effects on human cancer cells. Antiproliferative activity was found in direct correlation with the lipophilicity, while, a decrease in heterocycle number from benzodifuran to benzofuran derivatives further improved the antiproliferative effect. In fact, **BF1** emerged as the most interesting candidate as anticancer drug, being cytotoxic on PC-3 cells, ($IC_{50} = 33$ μM), selective with respect to non-cancerous cells and able to arrest cancer cell cycle in S-phase. In line with previous mechanistic studies reporting on a connection between antiproliferative properties of heteroaromatic compounds able to arrest cell cycle progression, and their G4 DNA binding ability, we have proven that **BF1** binds telomeric DNA, inducing conformational variations in tel_{22} G4 DNA structure with an affinity, determined by fluorescence spectroscopy, significantly higher than that found for the benzodifuran counterpart (**BDF1**), whose slight interaction with G4 DNA takes place only well above the physiological temperature, condition under which an induced positive CD peak at 325 nm appears in DNA spectrum. Overall, this study leads to the conclusion that both 4-nitrophenyl-functionalized benzofuran/difuran systems deserve deep attention as potential therapeutic drugs in the panorama of novel anticancer drug discovery. Thus, future efforts are expected to improve the biological properties of both families and, in particular, in case of benzofuran derivatives we aim to vary both phenyl moiety and benzofuran substituents to evaluate how these modifications will reflect on the biological properties of these new potential drugs.

Acknowledgments

We thank Prof. Antonio Roviello for his precious suggestions and the University of Naples "Federico II" for the grant "000005 ALTRI_DR_409_2017_Rec_Ateneo_prof_MARASCO", to D.M.

Appendix A. Supplementary data

Details regarding synthesis, characterization and ^{1}H NMR and ^{13}CNMR spectra of new compounds. Supplementary data to this article can be found online at https://doi.org/10.1016/j.ijbiomac.2018.09.153.

References

[1] N.A. McGrath, M. Brichacek, J.T. Njardarson, A graphical journey of innovative organic architectures that have improved our lives, J. Chem. Educ. 87 (2010) 1348–1349, https://doi.org/10.1021/ed1003806.
[2] M. Barra, M. Biasiucci, A. Cassinese, P. D'Angelo, A.C. Barone, A. Carella, A. Roviello, Direct current and alternating current electrical transport properties of regioregular poly[3-(4-alkoxyphenyl)-thiophenes], J. Appl. Phys. 102 (2007) 1–7, https://doi.org/10.1063/1.2809357.
[3] A. Carella, R. Centore, L. Mager, A. Barsella, A. Fort, Crosslinkable organic glasses with quadratic nonlinear optical activity, Org. Electron. Physics, Mater. Appl. 8 (2007) 57–62, https://doi.org/10.1016/j.orgel.2006.10.008.

[4] T.C. Parker, Seth R. Marder, Synthetic Methods in Organic Electronic and Photonic Materials: A Practical Guide, http://pubs.rsc.org/en/content/ebook/978-1-84973-986-3#!divbookcontent 2015, Accessed date: 1 June 2017.

[5] C. Wang, H. Dong, W. Hu, Y. Liu, D. Zhu, Semiconducting π-conjugated systems in field-effect transistors: a material odyssey of organic electronics, Chem. Rev. 112 (2012) 2208–2267, https://doi.org/10.1021/cr100380z.

[6] H. Khanam, Shamsuzzaman, Bioactive benzofuran derivatives: a review, Eur. J. Med. Chem. 97 (2015) 483–504, https://doi.org/10.1016/j.ejmech.2014.11.039.

[7] R. Desimone, K. Currie, S. Mitchell, J. Darrow, D. Pippin, Privileged structures: applications in drug discovery, Comb. Chem. High Throughput Screen. 7 (2004) 473–493, https://doi.org/10.2174/1386207043328544.

[8] S. Alper-Hayta, M. Arisoy, Ö. Temiz-Arpaci, I. Yildiz, E. Aki, S. Özkan, F. Kaynak, Synthesis, antimicrobial activity, pharmacophore analysis of some new 2-(substitutedphenyl/benzyl)-5-[(2-benzofuryl)carboxamido]benzoxazoles, Eur. J. Med. Chem. 43 (2008) 2568–2578, https://doi.org/10.1016/j.ejmech.2007.12.019.

[9] J.N. Soni, S.S. Soman, Synthesis and antimicrobial evaluation of amide derivatives of benzodifuran-2-carboxylic acid, Eur. J. Med. Chem. 75 (2014) 77–81, https://doi.org/10.1016/j.ejmech.2014.01.026.

[10] I. Hayakawa, R. Shioya, T. Agatsuma, H. Furukawa, S. Naruto, Y. Sugano, 4-Hydroxy-3-methyl-6-phenylbenzofuran-2-carboxylic acid ethyl ester derivatives as potent anti-tumor agents, Bioorg. Med. Chem. Lett. 14 (2004) 455–458, https://doi.org/10.1016/j.bmcl.2003.10.039.

[11] F. Xie, H. Zhu, H. Zhang, Q. Lang, L. Tang, Q. Huang, L. Yu, In vitro and in vivo characterization of a benzofuran derivative, a potential anticancer agent, as a novel Aurora B kinase inhibitor, Eur. J. Med. Chem. 89 (2015) 310–319, https://doi.org/10.1016/j.ejmech.2014.10.044.

[12] M. Thévenin, S. Thoret, P. Grellier, J. Dubois, Synthesis of polysubstituted benzofuran derivatives as novel inhibitors of parasitic growth, Bioorg. Med. Chem. 21 (2013) 4885–4892, https://doi.org/10.1016/j.bmc.2013.07.002.

[13] Y.-N. Wang, M.-F. Liu, W.-Z. Hou, R.-M. Xu, J. Gao, A.-Q. Lu, M.-P. Xie, L. Li, J.-J. Zhang, Y. Peng, L.-L. Ma, X.-L. Wang, J.-G. Shi, S.-J. Wang, Bioactive benzofuran derivatives from Cortex Mori Radicis, and their neuroprotective and analgesic activities mediated by mGluR1, Molecules 22 (2017) 236, https://doi.org/10.3390/MOLECULES22020236.

[14] D. Ashok, K. Sudershan, M. Khalilullah, Solvent-free microwave-assisted synthesis of *E*-(1)-(6-benzoyl-3,5-dimethylfuro[3′,2′:4,5]benzo[*b*]furan-2-yl)-3-(aryl)-2-propen-1-ones and their antibacterial activity, Green Chem. Lett. Rev. 5 (2012) 121–125, https://doi.org/10.1080/17518253.2011.584912.

[15] Z. Feng, S. Mohapatra, P.G. Klimko, M.R. Hellberg, J.A. May, C. Kelly, G. Williams, M.A. McLaughlin, N.A. Sharif, Novel benzodifuran analogs as potent 5-HT2Areceptor agonists with ocular hypotensive activity, Bioorg. Med. Chem. Lett. 17 (2007) 2998–3002, https://doi.org/10.1016/j.bmcl.2007.03.073.

[16] G.N. Roviello, V. Roviello, D. Musumeci, C. Pedone, Synthesis of a novel benzodifuran derivative and its molecular recognition of poly rA RNA, Biol. Chem. 394 (2013) 1235–1239, https://doi.org/10.1515/hsz-2013-0154.

[17] D. Musumeci, G.N. Roviello, G. Rigione, D. Capasso, S. Di Gaetano, C. Riccardi, V. Roviello, D. Montesarchio, Benzodifuran derivatives as potential antiproliferative agents: possible correlation between their bioactivity and aggregation properties, Chempluschem 82 (2017) 251–260, https://doi.org/10.1002/cplu.201600547.

[18] V. Bruno, A. Castaldo, R. Centore, A. Sirigu, F. Sarcinelli, M. Casalboni, R. Pizzoferrato, Second harmonic generation in polymers containing a new azo chromophore based on phenylnitrobenzoxazole, J. Polym. Sci. A Polym. Chem. 40 (2002) 1468–1475, https://doi.org/10.1002/pola.10224.

[19] K.R. Justin Thomas, A. Baheti, Fluorene based organic dyes for dye sensitised solar cells: structure–property relationships, Mater. Technol. 28 (2013) 71–87, https://doi.org/10.1179/1753555712Y.0000000036.

[20] A. Carella, F. Borbone, A. Roviello, G. Roviello, A. Tuzi, A. Kravinsky, R. Shikler, G. Cantele, D. Ninno, Benzodifuroxazinones, a new class of heteroacene molecules for possible applications in organic electronics: synthesis, electronic properties and crystal structure, Dyes Pigments 95 (2012) 116–125, https://doi.org/10.1016/j.dyepig.2012.03.033.

[21] P. Huang, J. Du, M.C. Biewer, M.C. Stefan, M.S. Sherburn, S. Isoda, K. Komatsu, K. Cho, L. Qiu, E. Borguet, S. Decurtins, S. Decurtins, M.C. Stefan, Developments of furan and benzodifuran semiconductors for organic photovoltaics, J. Mater. Chem. A 3 (2015) 6244–6257, https://doi.org/10.1039/C4TA07111E.

[22] F. Borbone, O. Tarallo, V. Roviello, U. Caruso, B. Pirozzi, A. Roviello, Novel rigid rod polymers from a thermal cyclization reaction, Eur. Polym. J. 63 (2015) 80–89, https://doi.org/10.1016/j.eurpolymj.2014.12.022.

[23] Kevin W. Anderson, Takashi Ikawa, Rachel E. Tundel, S.L. Buchwald, The Selective Reaction of Aryl Halides with KOH: Synthesis of Phenols, Aromatic Ethers, and Benzofurans, 2006https://doi.org/10.1021/JA0639719.

[24] X. Guo, R. Yu, H. Li, Z. Li, Iron-catalyzed tandem oxidative coupling and annulation: an efficient approach to construct polysubstituted benzofurans, J. Am. Chem. Soc. 131 (2009) 17387–17393, https://doi.org/10.1021/ja907568j.

[25] C. Li, Y. Zhang, P. Li, L. Wang, Palladium-catalyzed oxidative cyclization of 3-phenoxyacrylates: an approach to construct substituted benzofurans from phenols, J. Organomet. Chem. 76 (2011) 4692–4696, https://doi.org/10.1021/jo200317f.

[26] D. Yue, T. Yao, R.C. Larock, Synthesis of 2,3-disubstituted benzo[b]furans by the palladium-catalyzed coupling of o-iodoanisoles and terminal alkynes, followed by electrophilic cyclization, J. Organomet. Chem. 70 (2005) 10292–10296, https://doi.org/10.1021/jo051299c.

[27] F. Singh, T. Wirth, Hypervalent iodine mediated oxidative cyclization of *o*-hydroxystilbenes into benzo- and naphthofurans, Synthesis-Stuttgart 44 (2012) 1171–1177, https://doi.org/10.1055/s-0031-1290588.

[28] C.M.A. Alves, S. Naik, P.J.G. Coutinho, M.S.T. Gonalves, Novel DNA fluorescence probes based on *N*-[5-(11-functionalised-undecylamino)-9H-benzo[a]phenoxazin-9-ylidene]propan-1-aminium chlorides: synthesis and photophysical studies, Tetrahedron Lett. 52 (2011) 112–116, https://doi.org/10.1016/j.tetlet.2010.10.165.

[29] L. Huo, Y. Huang, B. Fan, X. Guo, Y. Jing, M. Zhang, Y. Li, J. Hou, Synthesis of a 4,8-dialkoxy-benzo[1,2-b:4,5-b′]difuran unit and its application in photovoltaic polymer, Chem. Commun. 48 (2012) 3318, https://doi.org/10.1039/c2cc17708k.

[30] T.J. King, C.E. Newall, 175. The chemistry of colour reactions. The craven reaction, J. Chem. Soc. (1965) 974, https://doi.org/10.1039/jr9650000974.

[31] G.A.R. Kon, O.L. Brady, M.D. Porter, R. Craven, Notes, J. Chem. Soc. (1931) 1604, https://doi.org/10.1039/jr9310001604.

[32] M. Obushak, Synthesis of heterocycles on the basic of arylation products of unsaturated compounds. Part 9. Dialkyl 2,6-diamino-4-arylfuro[2′,3′:4,5]benzo[b]furan-3,7-dicarboxylates from 2-aryl-1,4-benzoquinones and cyanoacetic esters, Pol. J. Chem. (2002) 1419–1424https://yadda.icm.edu.pl/baztech/element/bwmeta1.element.baztech-article-BUJ1-0021-0006, Accessed date: 1 June 2017.

[33] B.W. Carlson, L.L. Miller, Mechanism of the oxidation of NADH by quinones. energetics of one-electron and hydride routes, J. Am. Chem. Soc. 107 (1985) 479–485, https://doi.org/10.1021/ja00288a035.

[34] X.Y. Li, B.F. He, H.J. Luo, N.Y. Huang, W.Q. Deng, 3-Acyl-5-hydroxybenzofuran derivatives as potential anti-estrogen breast cancer agents: a combined experimental and theoretical investigation, Bioorg. Med. Chem. Lett. 23 (2013) 4617–4621, https://doi.org/10.1016/j.bmcl.2013.06.022.

[35] R. Weinlich, A. Oberst, H.M. Beere, D.R. Green, Necroptosis in development, inflammation and disease, Nat. Rev. Mol. Cell Biol. 18 (2017) 127–136, https://doi.org/10.1038/nrm.2016.149.

[36] D.R. McIlwain, T. Berger, T.W. Mak, Caspase functions in cell death and disease, Cold Spring Harb. Perspect. Biol. 5 (2013) 1–28, https://doi.org/10.1101/cshperspect.a008656.

[37] C.M. Incles, C.M. Schultes, H. Kempski, H. Koehler, L.R. Kelland, S. Neidle, A G-quadruplex telomere targeting agent produces p16-associated senescence and chromosomal fusions in human prostate cancer cells, Mol. Cancer Ther. 3 (2004) 1201–1206http://www.ncbi.nlm.nih.gov/pubmed/15486186, Accessed date: 28 August 2018.

[38] A.K. Khaw, M. Silasudjana, B. Banerjee, M. Suzuki, R. Baskar, M.P. Hande, Inhibition of telomerase activity and human telomerase reverse transcriptase gene expression by histone deacetylase inhibitor in human brain cancer cells, Mutat. Res. Fundam. Mol. Mech. Mutagen. 625 (2007) 134–144, https://doi.org/10.1016/j.mrfmmm.2007.06.005.

[39] C.J. Sherr, The pezcoller lecture: cancer cell cycles revisited, Cancer Res. (2000) 3689–3695http://www.ncbi.nlm.nih.gov/pubmed/10919634, Accessed date: 24 May 2018.

[40] L. De Boer, V. Oakes, H. Beamish, N. Giles, F. Stevens, M. Somodevilla-Torres, C. Desouza, B. Gabrielli, Cyclin A/cdk2 coordinates centrosomal and nuclear mitotic events, Oncogene 27 (2008) 4261–4268, https://doi.org/10.1038/onc.2008.74.

[41] Y.C. Tsai, H. Qi, C.P. Lin, R.K. Lin, J.E. Kerrigan, S.G. Rzuczek, E.J. Lavoie, J.E. Rice, D.S. Pilch, Y.L. Lyu, L.F. Liu, A G-quadruplex stabilizer induces M-phase cell cycle arrest, J. Biol. Chem. 284 (2009) 22535–22543, https://doi.org/10.1074/jbc.M109.020230.

[42] G. Zhou, X. Liu, Y. Li, S. Xu, C. Ma, X. Wu, Y. Cheng, Z. Yu, G. Zhao, Y. Chen, Telomere targeting with a novel G-quadruplex-interactive ligand BRACO-19 induces T-loop disassembly and telomerase displacement in human glioblastoma cells, Oncotarget 7 (2016) 14,925–39, https://doi.org/10.18632/oncotarget.7483.

[43] J.S. Hudson, L. Ding, V. Le, E. Lewis, D. Graves, Recognition and binding of human telomeric G-quadruplex DNA by unfolding protein 1, Biochemistry 53 (2014) 3347–3356, https://doi.org/10.1021/bi500351u.

[44] A. Ambrus, D. Chen, J. Dai, T. Bialis, R.A. Jones, D. Yang, Human telomeric sequence forms a hybrid-type intramolecular G-quadruplex structure with mixed parallel/antiparallel strands in potassium solution, Nucleic Acids Res. 34 (2006) 2723–2735, https://doi.org/10.1093/nar/gkl348.

[45] M.P. Fuggetta, A. De Mico, A. Cottarelli, F. Morelli, M. Zonfrillo, F. Ulgheri, P. Peluso, A. Mannu, F. Deligia, M. Marchetti, G. Roviello, A. Reyes Romero, A. Dömling, P. Spanu, Synthesis and enantiomeric separation of a novel spiroketal derivative: a potent human telomerase inhibitor with high in vitro anticancer activity, J. Med. Chem. 59 (2016) 9140–9149, https://doi.org/10.1021/acs.jmedchem.6b01046.

[46] A.K. Jain, V.V. Reddy, A. Paul, K. Muniyappa, S. Bhattacharya, Synthesis and evaluation of a novel class of G-quadruplex-stabilizing small molecules based on the 1,3-phenylene-bis(piperazinyl benzimidazole) system, Biochemistry 48 (2009) 10693–10704, https://doi.org/10.1021/bi9003815.

[47] M.A. Mendez, V.A. Szalai, Fluorescence of unmodified oligonucleotides: a tool to probe G-quadruplex DNA structure, Biopolymers 91 (2009) 841–850, https://doi.org/10.1002/bip.21268.

[48] A. Russo, P.L. Scognamiglio, R.P. Hong Enriquez, C. Santambrogio, R. Grandori, D. Marasco, A. Giordano, G. Scoles, S. Fortuna, In silico generation of peptides by replica exchange Monte Carlo: docking-based optimization of maltose-binding-protein ligands, PLoS One 10 (2015), e0133571. https://doi.org/10.1371/journal.pone.0133571.

[49] S. Gao, Y. Cao, Y. Yan, X. Xiang, X. Guo, Correlations between fluorescence emission and base stacks of nucleic acid G-quadruplexes, RSC Adv. 6 (2016) 94531–94538, https://doi.org/10.1039/C6RA21347B.